Analyst

Mannitol-induced gold nanoparticle aggregation for the ligand-free detection of viral particles

Journal:	*Analyst*
Manuscript ID	AN-ART-05-2019-000830.R2
Article Type:	Paper
Date Submitted by the Author:	23-Jul-2019
Complete List of Authors:	Mi, Xue; Michigan Technological University, Chemical Engineering Lucier, Ellie; Michigan Technological University, Chemical Engineering Turpeinen, Dylan; Michigan Technological University, Chemical Engineering Yeo, Eugenia; National University of Singapore, Biomedical Engineering Kah, James; National University of Singapore, Biomedical Engineering Heldt, Caryn; Michigan Technological University, Chemical Engineering

Mannitol-induced gold nanoparticle aggregation for the ligand-free detection of viral particles

Xue Mi[1], Ellie M. Lucier[1], Dylan G. Turpeinen[1], Eugenia Li Ling Yeo[2], James Chen Yong Kah[2,*], and Caryn L. Heldt[1,*]

[1]Department of Chemical Engineering, Michigan Technological University, USA

[2]Department of Biomedical Engineering, National University of Singapore, Singapore

[*]Co-corresponding authors: kah@nus.edu.sg and heldt@mtu.edu

Revision to Analyst

ABSTRACT:

Traditional virus detection methods require ligands that bind to either viral capsid proteins or viral nucleic acids. Ligands are typically antibodies or oligonucleotides and they are expensive, have limited chemical stability, and can only detect one specific type of virus at a time. Here, the biochemical surface properties of viruses are exploited for ligand-free, nonspecific virus detection. It has been found that the osmolyte mannitol can preferentially aggregate virus, while leaving proteins in solution. This led to the development of a ligand-free detection of virus using gold nanoparticle (AuNP) aggregation. Porcine parvovirus (PPV) was incubated with AuNPs and aggregation of the PPV-AuNP complex with mannitol was detected by dynamic light scattering (DLS). The lowest detectable concentration of PPV was estimated to be 10^5 MTT_{50}/mL, which is lower than standard antibody assays. PPV was also detected when swabbed from a dry surface and in the presence of a protein solution matrix. The enveloped bovine viral diarrhea virus (BVDV) was also detected using mannitol-induced aggregation of BVDV-coated AuNPs. The lowest detectable concentration of BVDV was estimated to be 10^6 MTT_{50}/mL. This demonstrates that gold nanoparticle aggregation can detect virus without the use of specific ligands.

KEYWORDS:

Gold nanoparticle aggregation, glycine, surface plasmon resonance, osmolyte, antibody

INTRODUCTION

The novel properties of gold nanoparticles (AuNPs) can be harnessed to create specialized sensors for biomolecules.[1-3] One class of biomolecule that has shown great promise for AuNPs detection are viral particles.[4-6] Viruses are unique colloids that consist of a protein capsid shell that encapsulate nucleic acids and may be surrounded by a lipid bilayer. Most commonly, the capsid proteins or nucleic acids are the biochemical targets for direct virus detection.[7-10] Virus can be detected with lateral flow assays, in which the AuNPs function as direct coloring,[11-12] or through the aggregation of the AuNPs.[3, 10, 13-14] While these are promising methods for disease detection of specific viral infections, there is a need to detect the presence of infectious virus particles without being virus specific. In one case, blood transfusions in Africa are commonly tested for only three different viruses, HIV, hepatitis B and hepatitis C,[15] whereas in the US, blood donations are tested for at least seven different viruses.[16] A general virus detection method could alleviate the need for low resource countries to test for specific viruses in blood donations. The goal is not a disease diagnosis, but the general safety of the blood supply.

Another application could be the evaluation of the cleanliness of a surface. One example would be the elimination of norovirus after a cruise ship outbreak. According to the Centers for Disease Control and Prevention (CDC), norovirus causes about 20 million people in the US to have acute gastroenteritis each year[17] and the virus can be transmitted through contact with contaminated food, water or surfaces. A rapid and inexpensive virus detection method could alleviate many of these transmissions through the testing of surface cleanliness.

AuNPs are widely used as a colorimetric detection mechanism due to their unique surface plasmon resonance (SPR) property. A strong optical absorbance peak of AuNPs is dependent on the size of AuNPs and also highly sensitive to inter-particle separations. Aggregation of AuNPs

results in a red-shift and peak broadening of the ultraviolet-visible (UV-Vis) absorption spectrum and an obvious color change from red to dark blue or gray.[18-19] However, this type of detection is not sensitive to lower degrees of aggregation and not suitable for the analysis of colored samples. To overcome the limitations of colorimetric assays by UV-Vis detection,[20-21] the light scattering properties of AuNPs have been used for biomolecule detections.[6, 14, 22] Light scattering-based assays have a lower limit of detection, up to four orders of magnitude, as compared to UV-Vis spectrophotometric-based AuNPs aggregation detection.[23] Light scattering methods may be required to detect pathogens, which can be infectious at very low concentrations.

There have been assays developed for the detection of proteins using AuNP aggregation. Proteins non-specifically adsorb to AuNPs, creating a protein corona[24-25] through a combination of hydrophobic interactions,[26] electrostatic interactions,[27] and co-ordinate binding between the thiol or amino groups of proteins and the AuNPs.[28-29] A protein concentration assay has been developed by determining the amount of protein needed to create a protein corona around an AuNPs that will protect the nanoparticle from salt-induced aggregation.[30] This demonstrates the application of a non-specific biomolecule concentration assay using AuNPs aggregation.

AuNPs can be easily conjugated with biomolecules, making them a good candidate for specific virus detection using antibodies or oligonucleotides. AuNPs conjugated with an antibody can sensitively detect the presence of the H3N2 influenza A virus with a detection limit of 7.8 hemagglutination units.[13] Hepatitis C virus (HCV) specific oligonucleotide-functionalized AuNPs were used to quantify HCV RNA in clinical samples by AuNPs aggregation with a limit of detection of 4.57 international units (IU)/μL.[10] However, these systems require an antibody or oligonucleotide that is specific to the virus of interest for detection. But what if we need to know

if any virus is present? To develop a non-specific viral particle assay based on AuNPs aggregation, methods to aggregate generic viral particles need to be explored.

Virus particles can aggregate in a variety of solution conditions through manipulation of pH, salt concentration, and osmolyte concentration. Viruses tend to form aggregates close to their isoelectric point (pI), where the net charge of the virus surface is neutral and the repulsive electrostatic forces on the virus surfaces are the lowest.[31] MS2, ΦX174, and PRD1 bacteriophage particles formed aggregates when the pH was lowered from 7 to near their pI of 4.[32] Viruses show different degrees of aggregation depending on salt types and concentration. A sodium chloride solution ranging from 0.5-4 M reversibly aggregated the hepatitis B surface antigen (HBsAg) virus-like particles (VLPs) into oligomeric particles, while 1-2 M ammonium sulfate irreversibly aggregated the VLPs.[33]

Osmolytes have been shown to preferentially aggregate both the non-enveloped porcine parvovirus (PPV) and enveloped Sindbis virus (SINV) while not aggregating bovine serum albumin (BSA) or lysozyme.[34-36] The hypothesis of why this aggregation occurs is based on the differences between virus and protein surface chemistry. Most osmolytes protect proteins from high osmotic stress, resulting in enhanced protein stability.[37] Osmolytes have a high affinity for water and a low affinity for the protein backbone.[38-39] Therefore, osmolytes are able to remove water molecules near hydrophobic residues on the protein surface.[40] To compensate for this change in free energy, the protein rearranges into a more compact structure.[37] Viruses tend to aggregate in this same situation due to two major differences between viruses and proteins: viruses have been shown to be more hydrophobic than proteins,[41-42] allowing more surface area to be dehydrated, and viruses are more rigid than proteins and cannot collapse to compensate for the free energy change. In response to the change in free energy, viruses aggregate.

In this study, PPV and bovine viral diarrhea virus (BVDV) were detected by comparing the aggregation of virus-coated AuNPs in mannitol solutions and sodium chloride solutions to BSA and thyroglobulin-coated AuNPs. PPV and BVDV were chosen to demonstrate the robustness of this general virus particle detection assay, as PPV is a small non-enveloped virus while BVDV is a larger, enveloped virus. Results indicate that virus and protein-coated nanoparticles can be distinguished by a difference in aggregate size measured by dynamic light scattering (DLS). Two proof-of-concept tests were conducted to determine if PPV could be detected in simulated applications. PPV was dried on a surface and then recovered by rubbing the area with a wet cotton swab. The reconstituted PPV was quantitatively measured with the developed AuNPs aggregation assay. PPV could also be quantitatively detected in different concentrations of BSA solution matrix, demonstrating the possible application in testing blood donations. These results indicate that ligand-free AuNPs aggregation may be a promising detection method for the presence of viral particles. This nonspecific virus detection method is promising for determining the presence of viruses in a blood transfusion sample or on a contaminated surface.

EXPERIMENTAL SECTION

Materials. Bovine serum albumin (BSA) (≥98%) and thyroglobulin from porcine thyroid gland were purchased from Sigma-Aldrich (St. Louis, MO). For synthesis of AuNPs, gold (III) chloride trihydrate ($HAuCl_4 \cdot 3H_2O$) (≥99.9%) and trisodium citrate (ACS grade, ≥99.0%) were purchased from Sigma-Aldrich. Potassium phosphate monobasic (molecular biology grade, ≥99.0%), sodium phosphate monobasic monohydrate (ACS grade, 98.0-102.0%), and sodium chloride (ACS grade, ≥99.0%) were a gift from Millipore Sigma (Burlington, MA). Sodium

phosphate dibasic heptahydrate (ACS grade, 98.0-102.0%), D-mannitol (≥ 98%), and glutaraldehyde solution (Grade I, 70% in H_2O) were purchased from Sigma-Aldrich. Phosphate buffered saline (PBS) (pH = 7.2) was purchased from Life Technologies (Grand Island, NY). Thiazolyl blue tetrazolium bromide (MTT) (98%) was purchased from Alfa Aesar (Haverhill, MA). All aqueous solutions or buffers were prepared using purified water with a resistivity of ≥18 MΩ·cm from a Nanopure filtration system (Thermo Scientific, Waltham, MA) and filtered with a 0.2 μm bottle top filter (VWR, Radnor, PA) or a 0.2 μm syringe filter (VWR) prior to use.

Virus titration and purification. Porcine kidney cells (PK-13, CRL-6489) and bovine turbinate cells (BT-1, CRL-1390) were purchased from ATCC. Porcine parvovirus (PPV) strain NADL-2, was a gift from Dr. Ruben Carbonell (North Carolina State University, Raleigh, NC). Bovine viral diarrhea virus (BVDV) strain NADL was purchased from USDA APHIS. PPV was propagated in PK-13 cells and BVDV was propagated in BT-1 cells. Both PPV and BVDV were titrated with an MTT assay, as described previously.[43-44] The MTT assay is a cell viability assay that can be correlated with viral infectivity. For purification of virus, PPV or BVDV was first dialyzed using a Biotech Cellulose Ester 1000 kDa dialysis tubing (Rancho Dominguez, CA) at 4°C for two days with two buffer exchanges in 4 mM phosphate buffer (pH 7.2). The dialyzed virus was then polished with an Econo-Pac 10DG desalting column (Hercules, CA).

Synthesis and characterization of AuNPs. The citrate-capped AuNPs were synthesized using the previously established citrate reduction method.[30] Briefly, a trisodium citrate solution was added to boiling hydrochloroauric acid ($HAuCl_4$) solution and kept boiling for 15 minutes. The boiling solution color was observed to turn from pale yellow to purple, followed by the formation of deep red AuNPs colloids. The AuNP colloidal solution was cooled to room temperature for further characterization.

The synthesized AuNPs were characterized by UV-Vis absorption spectroscopy, dynamic light scattering (DLS), and transmission electron microscopy (TEM). The AuNPs solution was transferred into one well of a 96-well plate and the UV-Vis absorption spectrum was measured from 400 – 900 nm wavelength with a Synergy Mx microplate reader (Winooski, VT). The AuNPs solution hydrodynamic diameter and zeta potential were measured with a Malvern Zetasizer Nano ZS (Worcestershire, United Kingdom). The morphology of the AuNPs was characterized with a JEOL JEM-2010 TEM (Peabody, MA) at 200 kV. The concentration of the AuNPs was determined by the molar extinction coefficient, which is related to the particle diameter, using a previously established method.[45] The synthesized AuNPs were prepared fresh and kept at room temperature until use. The AuNPs were washed once by re-suspending the AuNPs pellet into nanopure water after pelleting with an ST16R Centrifuge (Thermo Scientific, Asheville, NC) at 7,000 × *g* for 20 minutes and diluted to a final concentration of 3.5 nM for subsequent experiments.

Coating and characterization of virus-AuNPs complexes. Different concentrations of purified PPV, BVDV, BSA, or thyroglobulin were added to the 3.5 nM AuNPs for a final concentration of 1.75 nM AuNPs. The coated AuNPs were vortexed and rotated end-over-end for 20 hours on a Roto-shake Genie rocker (Bohemia, NY) at the maximum rotation speed and then centrifuged at 6,000 × *g* for 20 minutes. The coated AuNPs were characterized by UV-Vis spectroscopy and DLS. The coated AuNPs were resuspended in a 1 M mannitol or 1 M sodium chloride solution and characterized.

Prior to detection of coated AuNPs with the Malvern Zetasizer, the virus was inactivated according to university biosafety protocols. A 7.14 μL of 70% glutaraldehyde solution was added to 1 mL of coated AuNPs before and after osmolyte or salt treatment to make the final

solution concentration 0.5% glutaraldehyde. Each tube was incubated at room temperature for 2 hours and was measured with the Malvern Zetasizer.

To quantify the aggregation of AuNPs, the mean hydrodynamic diameter (D_H), was measured by DLS. The change in the hydrodynamic diameter after treatment (ΔD_H) was calculated by **Eq. 1**.

$$\Delta D_H = D_{H\ coated\ AuNPs\ after\ treatment} - D_{H\ coated\ AuNPs\ before\ treatment} \quad (1)$$

A high ΔD_H represents a high degree of aggregation of coated AuNPs by either osmolyte or salt treatment.

For TEM characterization, 8 log PPV, 8 log PPV-coated AuNPs, and 8 log PPV-coated AuNPs after 1 M mannitol aggregation were adsorbed to a plasma etched TEM copper grids (Carbon Type-B, 300 mesh) for 2 minutes and were negatively stained with a 2% uranyl acetate (Fisher Scientific) for 2 minutes. The morphology of the virus samples was imaged with a JEOL JEM-2010 TEM at 80 kV.

Proof-of-concept tests. To determine the effect of protein interference on the virus detection, 500 μL of PPV was spiked into the same volume of solution containing different concentrations of BSA in PBS. The diameter was measured by DLS before and after addition of 1 M mannitol.

To simulate testing a surface for virus contamination, a swab test was developed.[46-47] Five 20 μL droplets of purified PPV in PBS buffer were placed on a sterile petri dish and dried in the biosafety cabinet for 1 hour. After the droplets evaporated, 100 μL of PBS buffer was pipetted onto the surface. The surface was then swabbed with a sterile cotton swab in a horizontal, vertical and diagonal direction, five times for each direction. The cotton swab was

placed in a tube containing 800 μL PBS buffer, incubated for 10 minutes, vortexed for 10 seconds and incubated for an additional 10 minutes. Liquid retained in the swab was removed by pressing of the cotton against the tube wall. The diameter was measured by DLS before and after addition of 1 M mannitol.

Statistical analysis. Statistical analysis was performed using R statistical software. A two sample t-test assuming equal variances (estimate pooled variance) was employed for comparison of virus-coated AuNPs with protein-coated AuNPs to determine an analytical limit of detection. Statistically significant differences are indicated by an asterisk (*).

RESULTS AND DISCUSSION

Rationale of virus detection method. Traditional virus detection methods require the specific detection of either capsid proteins by antiviral antibodies[13-14] or viral nucleic acids by complementary oligonucleotides.[3, 10] While this is a reliable method to detect known viral contaminates, it will not detect unknown viral particles. This work is a proof-of-concept study demonstrating that the behavior of virus and AuNPs in osmolyte and salt solutions can be used for virus detection of general viral contamination, without targeting a specific virus.

Earlier work demonstrated that viral particles preferentially flocculate in the presence of osmolytes.[34-35] As described in the introduction, this is due to the hydrophobicity and rigidity of virus particles. Osmolytes dehydrate protein and virus surfaces. However, since viruses are more hydrophobic than proteins,[41-42] they aggregate when there is a loss of their hydrating layer. Thus, viruses aggregate when in the presence of high osmolyte concentrations, while proteins do not. This study will apply this knowledge to induce the aggregation of virus and detect that aggregation with AuNPs as a beacon. A cartoon of AuNPs aggregation to probe the presence of viral particles is shown in **Figure 1**. In the presence of osmolytes, virus-coated AuNPs aggregate

and a measurable size increase is observed. However, the aggregation is not detected when protein-coated AuNPs are in the presence of osmolyte solutions. Salts are known to induce the aggregation of AuNPs,[48-50] since electrolytes can neutralize repulsive forces arising from the surface charge of citrate-coated AuNPs, causing the AuNPs to aggregate.[51] Minimal aggregation was shown when the osmolytes mannitol and glycine contacted uncoated AuNPs (see **SI**). Viruses on the surface of AuNPs can stabilize the nanoparticles from salt-induced aggregation, likely with a similar mechanism that protein-coated AuNPs are stabilized from salt-induced aggregation.[30] The reaction of the coated AuNPs to salt-induced and osmolyte-induced aggregation allowed the virus-containing samples to be identified from the protein-only samples.

Synthesis and characterization of AuNPs. The characterization of synthesized and coated AuNPs can be found in **Figure 2**. Synthesized AuNPs formed a red colloidal solution and were monodisperse and uniform, as shown in **Figure 2A**. The AuNPs showed a mean zeta potential of -36 ± 3 mV, indicating the synthesized citrate-capped AuNPs were stable and negatively charged (**Figure 2B)**. The isolated AuNPs had an absorbance peak at 519 nm in the UV-Vis absorbance spectrum (**Figure 2C).** The PPV-coated AuNPs and the BSA-coated AuNPs had a red-shift of 6 nm in the peak wavelength, as compared to bare AuNPs. This demonstrated that the AuNPs were coated successfully.[52] Coating of AuNPs with PPV or BSA also increased the hydrodynamic diameter of the AuNPs, as shown in **Figure 2D**. The bare AuNPs had a mean hydrodynamic diameter of 15 ± 0.4 nm. When the AuNPs were coated with PPV or BSA, the hydrodynamic diameter increased according to the size of the coating molecule, PPV is 18-26 nm[53] and BSA is ~6.8 nm[54]. Both the red-shift in the UV-Vis spectrum and the increase in the size indicated the formation of a monolayer[25] on the AuNPs surface for either protein or virus.

For biosafety reasons, the PPV had to be inactivated before testing with DLS. It was confirmed that the size did not change for the BSA-coated AuNPs before and after crosslinking. It was also observed that the size of the coated nanoparticles prior to aggregating agent addition was as expected in **Figure 2D**, providing evidence that the crosslinking did not induce AuNPs aggregation.

Concentration dependence. It was difficult to compare the concentration of PPV and BSA. It was determined that the best way to compare the virus and protein would be to find a concentration of each that covered the same area on the AuNP assuming similar binding affinities. It was calculated that 1 nM BSA covered the same area on the AuNPs as 10^8 MTT_{50}/mL of PPV (see **SI**), which is the highest concentration of PPV that can be obtained from our virus propagation method. The calculation assumed that the structure of the virus or BSA did not change from the crystal structure size[53-54] and that there was a 1:1,000,000 ratio of infectious to non-infectious virus particles for the PPV.[55] A higher concentration range of BSA was also tested because it has been shown that 1 nM BSA is too low a concentration to form a protein monolayer on AuNPs[56-57] that can halt salt-induced aggregation.[51]

The mean hydrodynamic diameter (D_H) measured by DLS was used to quantify the size of AuNPs before coating, after coating, and after inducing aggregation with either mannitol or salt. ΔD_H designates the change in the size of coated AuNPs after induction of aggregation with either osmolyte or salt (**Eq. 1**). **Figure 3A** shows that PPV-coated AuNPs increase in size after 1 M mannitol aggregation. The aggregation of PPV-coated AuNPs in mannitol is likely due to the flocculation of PPV caused by mannitol.[34, 36] Higher concentrations of PPV, starting at 10^6 MTT_{50}/mL, reduced aggregation in NaCl due to the virus protecting the AuNPs from salt-induced aggregation, shown in **Figure 3B**. The calculated ΔD_H for PPV shows a linear trend

when plotted against the log of PPV titer when PPV has a concentration greater than 10^5 MTT_{50}/mL (**Figure 3C**). The change in D_H due to the mannitol-induced aggregation of PPV increased from 25 ± 2 nm to 61 ± 16 nm between 10^4 MTT_{50}/mL and 10^8 MTT_{50}/mL. The lowest concentration of virus that could be detected was estimated to be 10^6 MTT_{50}/mL, which is ~1 pM. This lowest detectable concentration is lower than standard antibody binding assays that detect virus,[58-60] which typically have a nanomolar detection limit.[61-62]

The size of BSA-coated AuNPs in mannitol was much smaller than PPV-coated AuNPs, as shown in **Figure 3**. This demonstrates that there is a clear difference between AuNPs aggregation with mannitol in the presence of PPV versus BSA, demonstrating mannitol aggregation as a potential method to detect the virus. BSA-coated AuNPs showed the same trend as PPV-coated AuNPs, in the presence of salt. However, BSA-coated AuNPs is less protected than PPV from 0-1 nM, if we assume 10^8 PPV is equal to 1 nM of BSA, as calculated based on the same coverage area in the **SI**. This is likely due to a difference in binding affinity for BSA and PPV. The size difference, ΔD_H, in BSA-coated AuNPs induced by mannitol as a function of protein concentration can be seen in **Figure 3F**. The size increase of BSA-coated AuNPs in 1 M mannitol had a ΔD_H value in the range of 19 ± 1 nm to 33 ± 8 nm for all protein concentrations studied. For PPV, the ΔD_H reached 61 ± 16 nm for the highest concentration studied. This difference is the main basis for determining the detection of virus versus proteins.

Thyroglobulin-coated AuNPs (see **SI** for UV-Vis and DLS confirmation of coating) were also tested for their ability to aggregate in mannitol and salt. Thyroglobulin is a major protein involved with iodine metabolism and is 12 nm[63] in size. The reference range for thyroglobulin concentration is serum is about 20 to 25 ng/mL[64] (equivalent to 30-38 nM). All tested concentrations of thyroglobulin-coated AuNPs protected the AuNPs from aggregation by NaCl,

shown in **Figure 3H**. The size increase of thyroglobulin-coated AuNPs in 1 M mannitol had a ΔD_H value in the range of 22 ± 1 nm to 35 ± 4 nm for all protein concentrations studied (**Figure 3I**). This ΔD_H is smaller than PPV-coated AuNPs in mannitol. This further demonstrated that there is a clear difference between AuNPs aggregation with mannitol when in the presence of PPV versus protein controls.

The aggregation profile of PPV-coated AuNPs compared with protein-coated AuNPs by 1 M NaCl is similar to the aggregation profile of human papillomaviruses (HPV) type 16 L1 VLPs-coated AuNPs compared with BSA-coated AuNPs induced by 70 mM NaCl.[65] Aggregation of AuNPs-coated VLPs was sharply decreased as VLPs concentration was increased, while BSA-coated AuNPs showed a flat trend for AuNPs aggregation by salt.[65] While changes in NaCl aggregation of virus-coated AuNPs may detect viral particles compared with BSA near 1 μM, our data suggests that mannitol aggregation is more quantitative and less susceptible to contaminating proteins in solution.

TEM images of PPV, PPV-coated AuNPs and PPV-coated AuNPs with 1 M mannitol are shown in **Figure 3J-L**, respectively. The size of PPV detected in the images falls into the reported size range for PPV of 18 - 26 nm.[53] **Figure 3K** confirmed the successful interaction of PPV with the AuNPs. **Figure 3L** showed aggregation of PPV-coated AuNPs in mannitol. This demonstrates that PPV-coated AuNPs aggregate in the presence of mannitol.

UV-Vis absorption spectrum was used as a secondary detection method for AuNPs aggregation, however, no significant difference between the red-shift for mannitol-induced aggregation for PPV and the red-shift for mannitol-induced aggregation for control BSA could be found (see **SI**). This is possibly due to the lack of sensitivity of the UV-Vis absorption

spectrum that is needed to identify the small differences in aggregation between mannitol-induced aggregates of PPV and AuNPs.

Application: virus detection in protein solution matrix. To determine the interference of proteins on virus detection using the AuNPs aggregation method, PPV was spiked into an equal volume of BSA solution with difference concentrations to keep a constant final virus concentration of $10^{8.3} \pm 10^{0.2}$ MTT_{50}/mL. **Figure 4A** shows the average size of PPV-coated AuNPs in different concentrations of BSA before and after mannitol-induced aggregation. PPV-coated AuNPs placed in BSA solutions had a significantly larger size than BSA-coated AuNPs alone (**Figure 4B**). The highest BSA concentration of 500 μM was chosen because it is the physiological concentration of albumin in serum.[66-67] The calculated average concentration from the AuNPs standard detection curve for PPV was $10^{8.5} \pm 10^{0.7}$ MTT_{50}/mL, which is within $\pm 10^{0.5}$ (MTT_{50}/mL) (the known MTT error) from the PPV titer determined with the MTT assay. This reproducibility across different BSA concentrations indicates that AuNP aggregation in mannitol could be a promising diagnostic for virus in a protein solution.

Application: evaluation of surface contamination. AuNPs aggregation in mannitol was used as a proof-of-concept test to detect viral contamination on a surface. PPV was allowed to dry on a petri dish and was then collected with a cotton swab, as shown in **Figure 5A**. PPV at a concentration of $10^{6.9} \pm 10^{0.2}$ MTT_{50}/mL was collected with this swab sampling method, achieving a 60 ± 23% virus recovery. **Figure 5B** shows the ΔD_H after induction with mannitol. Swabbed PPV had a significantly larger aggregation of AuNPs caused by mannitol as compared to BSA. To determine the concentration of swabbed PPV using the AuNPs aggregation method, the PPV titer was determined from the AuNPs standard curve determined in **Figure 3E**. The

calculated titer was within the error of the MTT assay. This reproducibility indicates that the comparison of AuNPs aggregation in mannitol can be a promising test for the cleanliness of a surface for viral contamination.

Nonspecific virus detection. To test the non-specificity of the AuNPs aggregation assay, an enveloped virus BVDV with a size of 40-60 nm[68] was detected by mannitol-induced AuNP aggregation. The confirmation of BVDV-coated AuNPs is in the **SI**. Using the same procedure as PPV and the control proteins, the mean D_H was used to quantify the size of AuNPs before coating, after coating, and after inducing aggregation with either mannitol or salt. **Figure 6A** shows that BVDV-coated AuNPs increase in size after 1 M mannitol addition. At a concentration of 10^5 BVDV MTT_{50}/mL or higher, the AuNPs were protected from salt-induced aggregation, as shown in **Figure 6B**. The ΔD_H due to the mannitol-induced aggregation of BVDV increased from 51 ± 13 nm to 165 ± 31 nm between 10^4 MTT_{50}/mL and 10^7 MTT_{50}/mL, as shown in **Figure 6C**. The lowest detectable concentration was estimated to be 10^4 MTT_{50}/mL for BVDV. BVDV was detectable at a lower concentration than PPV. This could be due to the BVDV being an enveloped virus, potentially increasing its affinity for AuNPs. Or the size ratio between the virus and the AuNP could be important. In this study, only 15 nm AuNPs were used with virus that were ~20 nm (PPV) and between 40-60 nm for BVDV. Future work will explore a larger range of virus to AuNP size ratios.

CONCLUSIONS

The aggregation of virus-coated AuNPs in mannitol can be detected by DLS and there is a linear increase in aggregate size with an increase in PPV concentration on a semi-log plot. This indicates the potential of quantitative detection of virus with this described AuNPs aggregation

method. The lowest detectable concentration of virus was estimated to be 10^5 MTT_{50}/mL, which is lower than standard antibody assays. The non-specific nature of this assay was tested by detecting the aggregation of BVDV-coated AuNPs in mannitol. The lowest detection concentration for BVDV was estimated to be 10^6 MTT_{50}/mL.

The AuNPs aggregation assay has the ability to determine the presence of virus in up to 500 μM of BSA quantitatively, used as a model contaminate in a protein-rich biological fluid. Also, PPV was detected quantitatively after it was swabbed from a dried sample on a petri dish. The developed ligand-free AuNPs aggregation method can determine the presence of virus within 24 hours, which is comparable or faster than current virus detection methods. This general virus detection method could be a quick, sensitive, inexpensive and portable method for detecting the presence of viral particles in low resource countries. Future work includes exploring additional viruses, reducing the time for the assay, and determining the ideal AuNP sizes and shape. The goal is to develop this assay into an early screening step for a viral infection in blood samples or cleanliness of a surface, which could help to control a viral disease outbreak.

ACKNOWLEDGEMENTS

The authors thank EMD Millipore for the gift of chemicals used in this work and the support of Jessica Brassard for some of the artwork. Financial support was received from NSF (CAREER-1451959 and 1159425) and the James and Lorna Mack Chair in Bioengineering.

REFERENCES

(1) Chang, T. J.; Wang, L. B.; Zhao, K. X.; Ge, Y.; He, M.; Li, G. Duplex Identification of Staphylococcus Aureus by Aptamer and Gold Nanoparticles. *J. Nanosci. Nanotechnol.* **2016,** *16* (6), 5513-5519, DOI: 10.1166/jnn.2016.11656.

(2) Xiong, L. H.; He, X. W.; Xia, J. J.; Ma, H. W.; Yang, F.; Zhang, Q.; Huang, D. N.; Chen, L.; Wu, C. L.; Zhang, X. M.; Zhao, Z.; Wan, C. S.; Zhang, R. L.; Cheng, J. Q. Highly Sensitive Naked-Eye Assay for Enterovirus 71 Detection Based on Catalytic Nanoparticle Aggregation and Immunomagnetic Amplification. *ACS Appl. Mater. Interfaces* **2017,** *9* (17), 14691-14699, DOI: 10.1021/acsami.7b02237.

(3) Dharanivasan, G.; Riyaz, S. U. M.; Jesse, D. M. I.; Muthuramalingam, T. R.; Rajendran, G.; Kathiravan, K. DNA Templated Self-Assembly of Gold Nanoparticle Clusters in the Colorimetric Detection of Plant Viral DNA Using a Gold Nanoparticle Conjugated Bifunctional Oligonucleotide Probe. *RSC Adv.* **2016,** *6* (14), 11773-11785, DOI: 10.1039/c5ra25559g.

(4) Kumvongpin, R.; Jearanaikool, P.; Wilailuckana, C.; Sae-ung, N.; Prasongdee, P.; Daduang, S.; Wongsena, M.; Boonsiri, P.; Kiatpathomchai, W.; Swangvaree, S. S.; Sandee, A.; Daduang, J. High Sensitivity, Loop-Mediated Isothermal Amplification Combined with Colorimetric Gold-Nanoparticle Probes for Visual Detection of High Risk Human Papillomavirus Genotypes 16 and 18. *J. Virol. Methods* **2016,** *234*, 90-95, DOI: 10.1016/j.jviromet.2016.04.008.

(5) Lee, C.; Gaston, M. A.; Weiss, A. A.; Zhang, P. Colorimetric Viral Detection Based on Sialic Acid Stabilized Gold Nanoparticles. *Biosens. Bioelectron.* **2013,** *42*, 236-241, DOI: 10.1016/j.bios.2012.10.067.

(6) Driskell, J. D.; Jones, C. A.; Tompkins, S. M.; Tripp, R. A. One-Step Assay for Detecting Influenza Virus Using Dynamic Light Scattering and Gold Nanoparticles. *Analyst* **2011,** *136* (15), 3083-3090, DOI: 10.1039/c1an15303j.

(7) Heidari, Z.; Rezatofighi, S. E.; Rastegarzadeh, S. A Novel Unmodified Gold Nanoparticles-Based Assay for Direct Detection of Unamplified Bovine Viral Diarrhea Virus-Rna. *J. Nanosci. Nanotechnol.* **2016,** *16* (12), 12344-12350, DOI: 10.1166/jnn.2016.13752.

(8) Wang, L.; Liu, Z. M.; Xia, X. Y.; Huang, J. Y. Visual Detection of Maize Chlorotic Mottle Virus by Asymmetric Polymerase Chain Reaction with Unmodified Gold Nanoparticles as the Colorimetric Probe. *Anal. Methods* **2016,** *8* (38), 6959-6964, DOI: 10.1039/c6ay02116f.

(9) Poonthiyil, V.; Nagesh, P. T.; Husain, M.; Golovko, V. B.; Fairbanks, A. J. Gold Nanoparticles Decorated with Sialic Acid Terminated Bi-Antennary N-Glycans for the Detection of Influenza Virus at Nanomolar Concentrations. *Chemistryopen* **2015,** *4* (6), 708-716, DOI: 10.1002/open.201500109.

(10) Shawky, S. M.; Awad, A. M.; Allam, W.; Alkordi, M. H.; El-Khamisy, S. F. Gold Aggregating Gold: A Novel Nanoparticle Biosensor Approach for the Direct Quantification of Hepatitis C Virus Rna in Clinical Samples. *Biosens. Bioelectron.* **2017,** *92*, 349-356, DOI: 10.1016/j.bios.2016.11.001.

(11) Hwang, S. G.; Ha, K.; Guk, K.; Lee, D. K.; Eom, G.; Song, S.; Kang, T.; Park, H.; Jung, J.; Lim, E. K. Rapid and Simple Detection of Tamiflu-Resistant Influenza Virus: Development of

Oseltamivir Derivative-Based Lateral Flow Biosensor for Point-of-Care (Poc) Diagnostics. *Sci. Rep.* **2018,** *8*, DOI: 10.1038/s41598-018-31311-x.

(12) Wu, J. C.; Chen, C. H.; Fu, J. W.; Yang, H. C. Electrophoresis-Enhanced Detection of Deoxyribonucleic Acids on a Membrane-Based Lateral Flow Strip Using Avian Influenza H5 Genetic Sequence as the Model. *Sensors* **2014,** *14* (3), 4399-4415, DOI: 10.3390/s140304399.

(13) Liu, Y. J.; Zhang, L. Q.; Wei, W.; Zhao, H. Y.; Zhou, Z. X.; Zhang, Y. J.; Liu, S. Q. Colorimetric Detection of Influenza a Virus Using Antibody-Functionalized Gold Nanoparticles. *Analyst* **2015,** *140* (12), 3989-3995, DOI: 10.1039/c5an00407a.

(14) Lai, Y. H.; Koo, S.; Oh, S. H.; Driskell, E. A.; Driskell, J. D. Rapid Screening of Antibody-Antigen Binding Using Dynamic Light Scattering (Dls) and Gold Nanoparticles. *Anal. Methods* **2015,** *7* (17), 7249-7255, DOI: 10.1039/c5ay00674k.

(15) Prugger, C.; Laperche, S.; Murphy, E. L.; Bloch, E. M.; Kaidarova, Z.; Tafflet, M.; Lefrere, J. J.; Jouven, X. Screening for Transfusion Transmissible Infections Using Rapid Diagnostic Tests in Africa: A Potential Hazard to Blood Safety? *Vox Sang.* **2016,** *110* (2), 196-8, DOI: 10.1111/vox.12327.

(16) FDA Complete List of Donor Screening Assays for Infectious Agents and Hiv Diagnostic Assays. https://www.fda.gov/BiologicsBloodVaccines/BloodBloodProducts/ApprovedProducts/LicensedProductsBLAs/BloodDonorScreening/InfectiousDisease/ucm080466.htm.

(17) CDC Prevent the Spread of Norovirus. https://www.cdc.gov/features/norovirus/index.html.

(18) Park, J.-E.; Kim, K.; Jung, Y.; Kim, J.-H.; Nam, J.-M. Metal Nanoparticles for Virus Detection. *ChemNanoMat* **2016,** *2* (10), 927-936, DOI: 10.1002/cnma.201600165.

(19) Radwan, S.; Azzazy, H. M. E. Gold Nanoparticles for Molecular Diagnostics. *Expert Rev. Mol. Diagn.* **2009,** *9* (5), 511-524, DOI: 10.1586/erm.09.33.

(20) Jans, H.; Liu, X.; Austin, L.; Maes, G.; Huo, Q. Dynamic Light Scattering as a Powerful Tool for Gold Nanoparticle Bioconjugation and Biomolecular Binding Studies. *Anal. Chem.* **2009,** *81* (22), 9425-9432, DOI: 10.1021/ac901822w.

(21) Ling, J.; Huang, C. Z.; Li, Y. F.; Zhang, L.; Chen, L. Q.; Zhen, S. J. Light-Scattering Signals from Nanoparticles in Biochemical Assay, Pharmaceutical Analysis and Biological Imaging. *Trac-Trends in Anal. Chem.* **2009,** *28* (4), 447-453, DOI: 10.1016/j.trac.2009.01.003.

(22) Wang, X. H.; Li, Y.; Quan, D. Q.; Wang, J. D.; Zhang, Y. H.; Du, J.; Peng, J. C.; Fu, Q. X.; Zhou, Y.; Jia, S. Z.; Wang, Y. L.; Zhan, L. S. Detection of Hepatitis B Surface Antigen by Target-Induced Aggregation Monitored by Dynamic Light Scattering. *Anal. Biochem.* **2012,** *428* (2), 119-125, DOI: 10.1016/j.ab.2012.06.011.

(23) Storhoff, J. J.; Lucas, A. D.; Garimella, V.; Bao, Y. P.; Müller, U. R. Homogeneous Detection of Unamplified Genomic DNA Sequences Based on Colorimetric Scatter of Gold Nanoparticle Probes. *Nat. Biotechnol.* **2004,** *22*, 883, DOI: 10.1038/nbt977.

(24) Sanchez-Pomales, G.; Morris, T. A.; Falabella, J. B.; Tarlov, M. J.; Zangmeister, R. A. A Lectin-Based Gold Nanoparticle Assay for Probing Glycosylation of Glycoproteins. *Biotechnol. Bioeng.* **2012,** *109* (9), 2240-2249, DOI: 10.1002/bit.24513.

(25) Ho, Y. T.; Poinard, B.; Yeo, E. L. L.; Kah, J. C. Y. An Instantaneous Colorimetric Protein Assay Based on Spontaneous Formation of a Protein Corona on Gold Nanoparticles. *Analyst* **2015,** *140* (4), 1026-1036, DOI: 10.1039/c4an01819b.

(26) Dominguez-Medina, S.; Blankenburg, J.; Olson, J.; Landes, C. F.; Link, S. Adsorption of a Protein Mono Layer Via Hydrophobic Interactions Prevents Nanoparticle Aggregation under

Harsh Environmental Conditions. *ACS Sustainable Chem. Eng.* **2013,** *1* (7), 833-842, DOI: 10.1021/sc400042h.

(27) Wang, A. L.; Perera, Y. R.; Davidson, M. B.; Fitzkee, N. C. Electrostatic Interactions and Protein Competition Reveal a Dynamic Surface in Gold Nanoparticle-Protein Adsorption. *J. Phys. Chem. C* **2016,** *120* (42), 24231-24239, DOI: 10.1021/acs.jpcc.6b08469.

(28) Johnston, B. D.; Kreyling, W. G.; Pfeiffer, C.; Schaffler, M.; Sarioglu, H.; Ristig, S.; Hirn, S.; Haberl, N.; Thalhammer, S.; Hauck, S. M.; Semmler-Behnke, M.; Epple, M.; Huhn, J.; Del Pino, P.; Parak, W. J. Colloidal Stability and Surface Chemistry Are Key Factors for the Composition of the Protein Corona of Inorganic Gold Nanoparticles. *Adv. Funct. Mater.* **2017,** *27* (42), 9, DOI: 10.1002/adfm.201701956.

(29) Burt, J. L.; Gutierrez-Wing, C.; Miki-Yoshida, M.; Jose-Yacaman, M. Noble-Metal Nanoparticles Directly Conjugated to Globular Proteins. *Langmuir* **2004,** *20* (26), 11778-11783, DOI: 10.1021/la048287r.

(30) Yeo, E. L. L.; Parthasarathy, K.; Yeo, H.; Ng, M. Understanding Aggregation-Based Assays: Nature of Protein Corona and Number of Epitopes on Antigen Matters. *RSC Adv.* **2015,** *5* (20), 14982-14993, DOI: 10.1039/C4RA12089B.

(31) Michen, B.; Graule, T. Isoelectric Points of Viruses. *J. Appl. Microbiol.* **2010,** *109* (2), 388-397, DOI: 10.1111/j.1365-2672.2010.04663.x.

(32) Dika, C.; Duval, J. F. L.; Francius, G.; Perrin, A.; Gantzer, C. Isoelectric Point Is an Inadequate Descriptor of Ms2, Phi X 174 and Prd1 Phages Adhesion on Abiotic Surfaces. *J. Colloid Interface Sci.* **2015,** *446*, 327-334, DOI: 10.1016/j.jcis.2014.08.055.

(33) Chen, Y.; Zhang, Y.; Quan, C.; Luo, J.; Yang, Y. L.; Yu, M. R.; Kong, Y. J.; Ma, G. H.; Su, Z. G. Aggregation and Antigenicity of Virus Like Particle in Salt Solution-a Case Study with

Hepatitis B Surface Antigen. *Vaccine* **2015,** *33* (35), 4300-4306, DOI: 10.1016/j.vaccine.2015.03.078.

(34) Gencoglu, M. F.; Pearson, E.; Heldt, C. L. Porcine Parvovirus Flocculation and Removal in the Presence of Osmolytes. *J. Biotechnol.* **2014,** *186*, 83-90, DOI: 10.1016/j.jbiotec.2014.06.011.

(35) Gencoglu, M.; Heldt, C. Enveloped Virus Flocculation and Removal in Osmolyte Solutions. *J. Biotechnol.* **2015,** *206*, 8-11, DOI: 10.1016/j.jbiotec.2015.03.030.

(36) Heldt, C. L.; Saksule, A.; Joshi, P. U.; Ghafarian, M. A Generalized Purification Step for Viral Particles Using Mannitol Flocculation. *Biotechnol. Prog.* **2018,** *34* (4), 1027-1035, DOI: 10.1002/btpr.2651.

(37) Godawat, R.; Jamadagni, S. N.; Garde, S. Characterizing Hydrophobicity of Interfaces by Using Cavity Formation, Solute Binding, and Water Correlations. *Proc. Natl. Acad. Sci. U. S. A.* **2009,** *106* (36), 15119-15124, DOI: 10.1073/pnas.0902778106.

(38) Hu, C. Y.; Pettitt, B. M.; Roesgen, J. Osmolyte Solutions and Protein Folding. *F1000 Biol. Rep.* **2009,** *1*, 41, DOI: 10.3410/B1-41.

(39) Bolen, D. W. Effects of Naturally Occurring Osmolytes on Protein Stability and Solubility: Issues Important in Protein Crystallization. *Methods* **2004,** *34* (3), 312-322, DOI: 10.1016/j.ymeth.2004.03.022.

(40) Patel, A. J.; Varilly, P.; Jamadagni, S. N.; Hagan, M. F.; Chandler, D.; Garde, S. Sitting at the Edge: How Biomolecules Use Hydrophobicity to Tune Their Interactions and Function. *J. Phys. Chem. B* **2012,** *116* (8), 2498-503, DOI: 10.1021/jp2107523.

(41) Heldt, C. L.; Zahid, A.; Vijayaragavan, K. S.; Mi, X. Experimental and Computational Surface Hydrophobicity Analysis of a Non-Enveloped Virus and Proteins. *Colloids Surf., B* **2017,** *153*, 77-84, DOI: 10.1016/j.colsurfb.2017.02.011.

(42) Johnson, S. A.; Walsh, A.; Brown, M. R.; Lute, S. C.; Roush, D. J.; Burnham, M. S.; Brorson, K. A. The Step-Wise Framework to Design a Chromatography-Based Hydrophobicity Assay for Viral Particles. *J. Chromatogr. B* **2017,** *1061-1062*, 430-437, DOI: 10.1016/j.jchromb.2017.08.002.

(43) Tafur, M. F.; Vijayaragavan, K. S.; Heldt, C. L. Reduction of Porcine Parvovirus Infectivity in the Presence of Protecting Osmolytes. *Antiviral Res.* **2013,** *99* (1), 27-33, DOI: 10.1016/j.antiviral.2013.04.019.

(44) Meng, H.; Forooshani, P. K.; Joshi, P. U.; Osborne, J.; Mi, X.; Meingast, C.; Pinnaratip, R.; Kelley, J.; Narkar, A.; He, W. et al. Biomimetic Recyclable Microgels for on-Demand Generation of Hydrogen Peroxide and Antipathogenic Application. *Acta Biomater.* **2019**, *83*, 109-118, DOI: 10.1016/j.actbio.2018.10.037.

(45) Haiss, W.; Thanh, N. T. K.; Aveyard, J.; Fernig, D. Determination of Size and Concentration of Gold Nanoparticles from UV-Vis Spectra. *Anal. Chem.* **2007,** *79* (11), 4215-4221, DOI: 10.1021/ac0702084.

(46) Scherer, K.; Made, D.; Ellerbroek, L.; Schulenburg, J.; Johne, R.; Klein, G. Application of a Swab Sampling Method for the Detection of Norovirus and Rotavirus on Artificially Contaminated Food and Environmental Surfaces. *Food Environ. Virol.* **2009,** *1* (1), 42-49, DOI: 10.1007/s12560-008-9007-0.

(47) Park, G. W.; Chhabra, P.; Vinje, J. Swab Sampling Method for the Detection of Human Norovirus on Surfaces. *J. Visualized Exp.* **2017,** (120), DOI: 10.3791/55205.

(48) Christau, S.; Moeller, T.; Genzer, J.; Koehler, R.; von Klitzing, R. Salt-Induced Aggregation of Negatively Charged Gold Nanoparticles Confined in a Polymer Brush Matrix. *Macromolecules* **2017,** *50* (18), 7333-7343, DOI: 10.1021/acs.macromol.7b00866.

(49) Sun, M. M.; Liu, F.; Zhu, Y. K.; Wang, W. S.; Hu, J.; Liu, J.; Dai, Z. F.; Wang, K.; Wei, Y.; Bai, J.; Gao, W. P. Salt-Induced Aggregation of Gold Nanoparticles for Photoacoustic Imaging and Photothermal Therapy of Cancer. *Nanoscale* **2016,** *8* (8), 4452-4457, DOI: 10.1039/c6nr00056h.

(50) Han, X. G.; Goebl, J.; Lu, Z. D.; Yin, Y. D. Role of Salt in the Spontaneous Assembly of Charged Gold Nanoparticles in Ethanol. *Langmuir* **2011,** *27* (9), 5282-5289, DOI: 10.1021/la200459t.

(51) Pamies, R.; Cifre, J. G. H.; Espin, V. F.; Collado-Gonzalez, M.; Banos, F. G. D.; de la Torre, J. G. Aggregation Behaviour of Gold Nanoparticles in Saline Aqueous Media. *J. Nanopart. Res.* **2014,** *16* (4), DOI: 10.1007/s11051-014-2376-4.

(52) Kah, J. C. Y.; Kho, K. W.; Lee, C. G. L.; Sheppard, C. J. R.; Shen, Z. X.; Soo, K. C.; Olivo, M. C. Early Diagnosis of Oral Cancer Based on the Surface Plasmon Resonance of Gold Nanoparticles. *Int. J. Nanomed.* **2007,** *2* (4), 785-798.

(53) Norkin, L. C. *Virology: Molecular Biology and Pathogenesis*, ASM Press: 2010.

(54) Flecha, F. L. G.; Levi, V. Determination of the Molecular Size of Bsa by Fluorescence Anisotropy. *Biochem. Mol. Biol. Educ.* **2003,** *31* (5), 319-322, DOI: 10.1002/bmb.2003.494031050261.

(55) Muzyczka, N.; Berns, K. I. Parvoviridae: The Viruses and Their Replication. In *Field's Virology*; Knipe, D. M.; Howely, P. M., Eds.; Lippincott Williams & Wilkins: 2001; pp 2327-59.

(56) Davidson, A. M.; Brust, M.; Cooper, D. L.; Volk, M. Sensitive Analysis of Protein Adsorption to Colloidal Gold by Differential Centrifugal Sedimentation. *Anal. Chem.* **2017**, *89* (12), 6807-6814, DOI: 10.1021/acs.analchem.7b01229.

(57) Lacerda, S. H. D. P.; Park, J. J.; Meuse, C.; Pristinski, D.; Becker, M. L.; Karim, A.; Douglas, J. F. Interaction of Gold Nanoparticles with Common Human Blood Proteins. *ACS nano* **2009**, *4* (1), 365-379, DOI: 10.1021/nn9011187.

(58) Rivera, E.; Sjoland, L.; Karlsson, K. A. A Solid-Phase Fluorescent Immunoassay for the Rapid Detection of Virus-Antigen or Antibodies in Fetuses Infected with Porcine Parvovirus. *Arch. Virol.* **1986,** *88* (1-2), 19-26, DOI: 10.1007/bf01310886.

(59) Csagola, A.; Zadori, Z.; Meszaros, I.; Tuboly, T. Detection of Porcine Parvovirus 2 (Ungulate Tetraparvovirus 3) Specific Antibodies and Examination of the Serological Profile of an Infected Swine Herd. *Plos One* **2016,** *11* (3), DOI: 10.1371/journal.pone.0151036.

(60) Westenbrink, F.; Veldhuis, M. A.; Brinkhof, J. M. A. An Enzyme-Linked Immunosorbent-Assay for Detection of Antibodies to Porcine Parvovirus. *J. Virol. Methods* **1989,** *23* (2), 169-178, DOI: 10.1016/0166-0934(89)90130-4.

(61) Brinker, C. J.; Cao, G. Annual Review of Nano Research, World Scientific: 2010; Vol. 3, pp 50.

(62) Chen, L.; Neethirajan, S. A Homogenous Fluorescence Quenching Based Assay for Specific and Sensitive Detection of Influenza Virus a Hemagglutinin Antigen. *Sensors* **2015**, *15* (4), 8852-8865, DOI: 10.3390/s150408852.

(63) Schön, P.; Degefa, T. H.; Asaftei, S.; Meyer, W.; Walder, L. Charge Propagation in "Ion Channel Sensors" Based on Protein-Modified Electrodes and Redox Marker Ions. *J. Am. Chem. Soc.* **2005**, *127* (32), 11486-11496, DOI: 10.1021/ja051574c.

(64) Indrasena, B. S. H. Use of Thyroglobulin as a Tumour Marker. *World journal of biological chemistry* **2017**, *8* (1), 81, DOI: 10.4331/wjbc.v8.i1.81.

(65) Palomino-Vizcaino, G.; Resendiz, D. G. V.; Benitez-Hess, M. L.; Martinez-Acuna, N.; Tapia-Vieyra, J. V.; Bahena, D.; Diaz-Sanchez, M.; Garcia-Gonzalez, O. P.; Alvarez-Sandoval, B. A.; Alvarez-Salas, L. M. Effect of HPV16 L1 Virus-Like Particles on the Aggregation of Non-Functionalized Gold Nanoparticles. *Biosens. Bioelectron.* **2018,** *100*, 176-183, DOI: 10.1016/j.bios.2017.09.001.

(66) Peters Jr, T. *All About Albumin: Biochemistry, Genetics, and Medical Applications*, Academic press: 1995.

(67) Choi, S.; Choi, E. Y.; Kim, D. J.; Kim, J. H.; Kim, T. S.; Oh, S. W. A Rapid, Simple Measurement of Human Albumin in Whole Blood Using a Fluorescence Immunoassay (I). *Clin. Chim. Acta* **2004**, *339* (1-2), 147-156, DOI: 10.1016/j.cccn.2003.10.002.

(68) Kim, I. S.; Choi, Y. W.; Lee, S. R. Optimization and Validation of a Virus Filtration Process for Efficient Removal of Viruses from Urokinase Solution Prepared from Human Urine. *J. Microbiol. Biotechnol.* **2004**, *14* (1), 140-147.

FIGURE CAPTIONS

Figure 1 The outcome of AuNPs aggregation detection of virus

Figure 2 Characterization of synthesized and coated AuNPs. (A) TEM image of the AuNPs, the inset image showing the color of synthesized AuNPs, (B) zeta potential, (C) UV-Vis absorption spectrum, (D) hydrodynamic diameter

Figure 3 Concentration dependence for detection of PPV versus control BSA & thyroglobulin. (A&D&G) Size profile of PPV, BSA or thyroglobulin coated AuNPs as a function of concentrations before and after 1 M mannitol addition as measured by DLS. (B&E&H) Size profile of PPV, BSA or thyroglobulin coated AuNPs as a function of concentrations after 1 M NaCl addition as measured by DLS. (C&F&I) Change in AuNPs aggregation size for PPV, BSA or thyroglobulin after 1 M mannitol addition. Solid markers represent PPV, open markers represent BSA and thyroglobulin. All data points are the average of three separate tests and error bars represent the standard deviation. Concentrations are plotted as a log scale. TEM images of (J) 8 log PPV, (K) 8 log PPV-coated AuNPs and (L) 8 log PPV-coated AuNPs with 1 M mannitol. *$p < 0.05$ for virus compared to BSA and thyroglobulin controls.

Figure 4 Detection of virus in a protein solution matrix. (A) The average size of PPV-coated AuNPs in different concentrations of BSA before and after 1 M mannitol addition and measured by DLS. (B) The change in the size of PPV-coated AuNPs in different concentrations of BSA after 1 M mannitol addition. Solid symbols represent PPV and open symbols represent BSA only. All data points are the average of three separate tests and error bars represent the standard deviation.

Figure 5 Swab sampling to detect contamination of PPV on a surface. (A) The process of swab sampling, (B) Size aggregation measured by DLS for swabbed PPV versus control swabbed BSA. Swabbed PPV is $10^{6.9} \pm 10^{0.2}$ MTT_{50}/mL as measured by the MTT assay and $10^{7.4}$ MTT_{50}/mL as measured by the PPV-AuNPs aggregation assay in 1 M mannitol. All data points are the average of three separate tests and error bars represent the standard deviation.

Figure 6 Concentration dependence for detection of BVDV. (A) Size profile of BVDV coated AuNPs as a function of concentrations before and after 1 M mannitol addition as measured by DLS. (B) Size profile of BVDV coated AuNPs as a function of concentrations after 1 M NaCl addition as measured by DLS. (C) Change in AuNPs aggregation size for BVDV after 1 M mannitol addition. All data points are the average of three separate tests and error bars represent

the standard deviation. *$p < 0.05$ for virus compared to BSA and thyroglobulin controls in Figure 3.

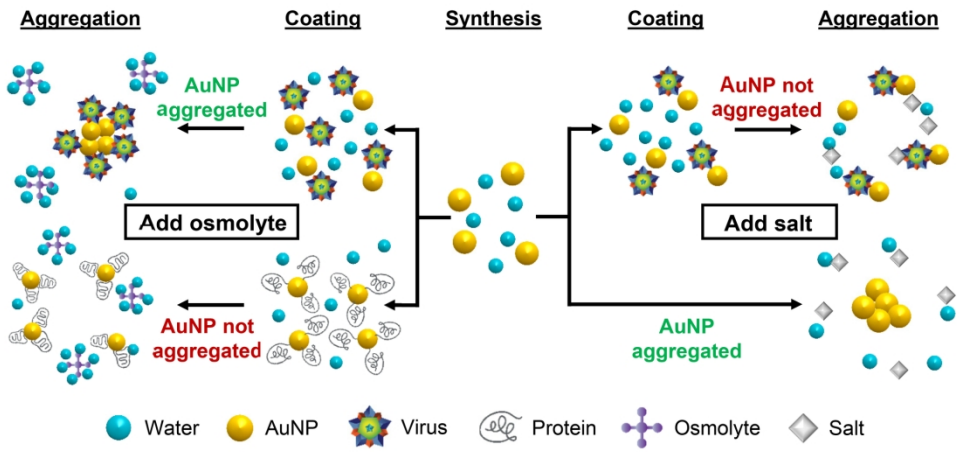

Figure 1 The outcome of AuNPs aggregation detection of virus

189x95mm (300 x 300 DPI)

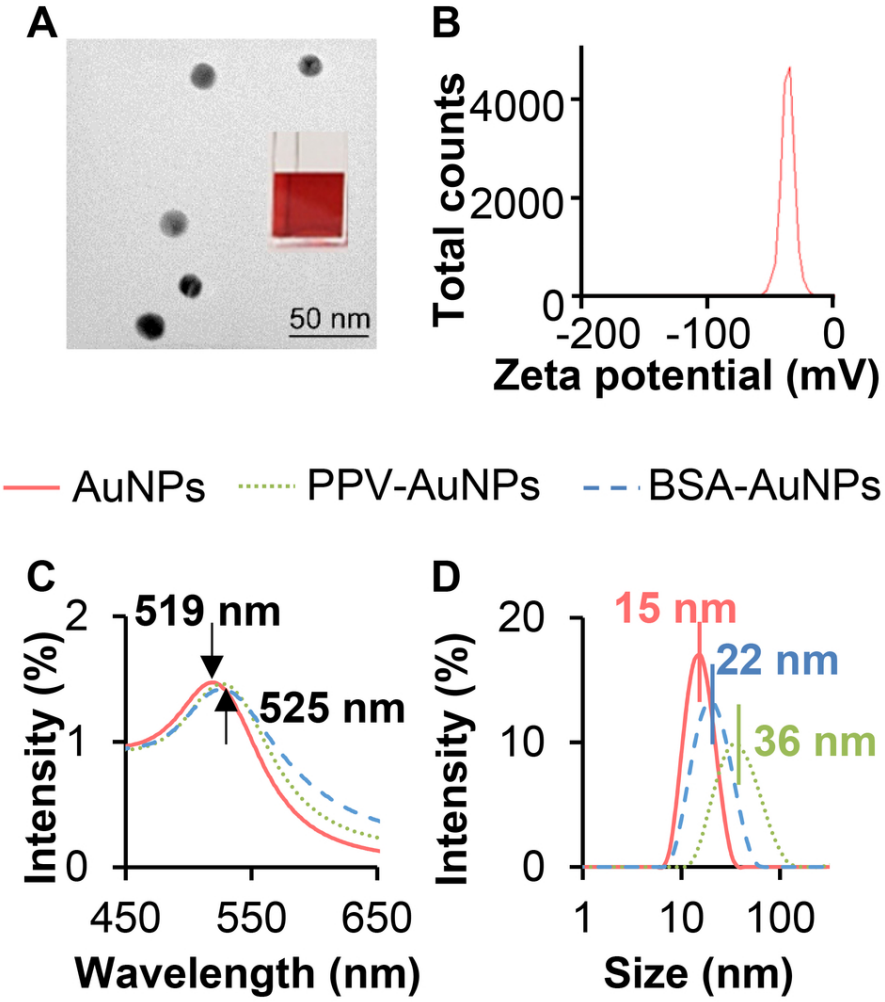

Figure 2 Characterization of synthesized and coated AuNPs. (A) TEM image of the AuNPs, the inset image showing the color of synthesized AuNPs, (B) zeta potential, (C) UV-Vis absorption spectrum, (D) hydrodynamic diameter

90x95mm (300 x 300 DPI)

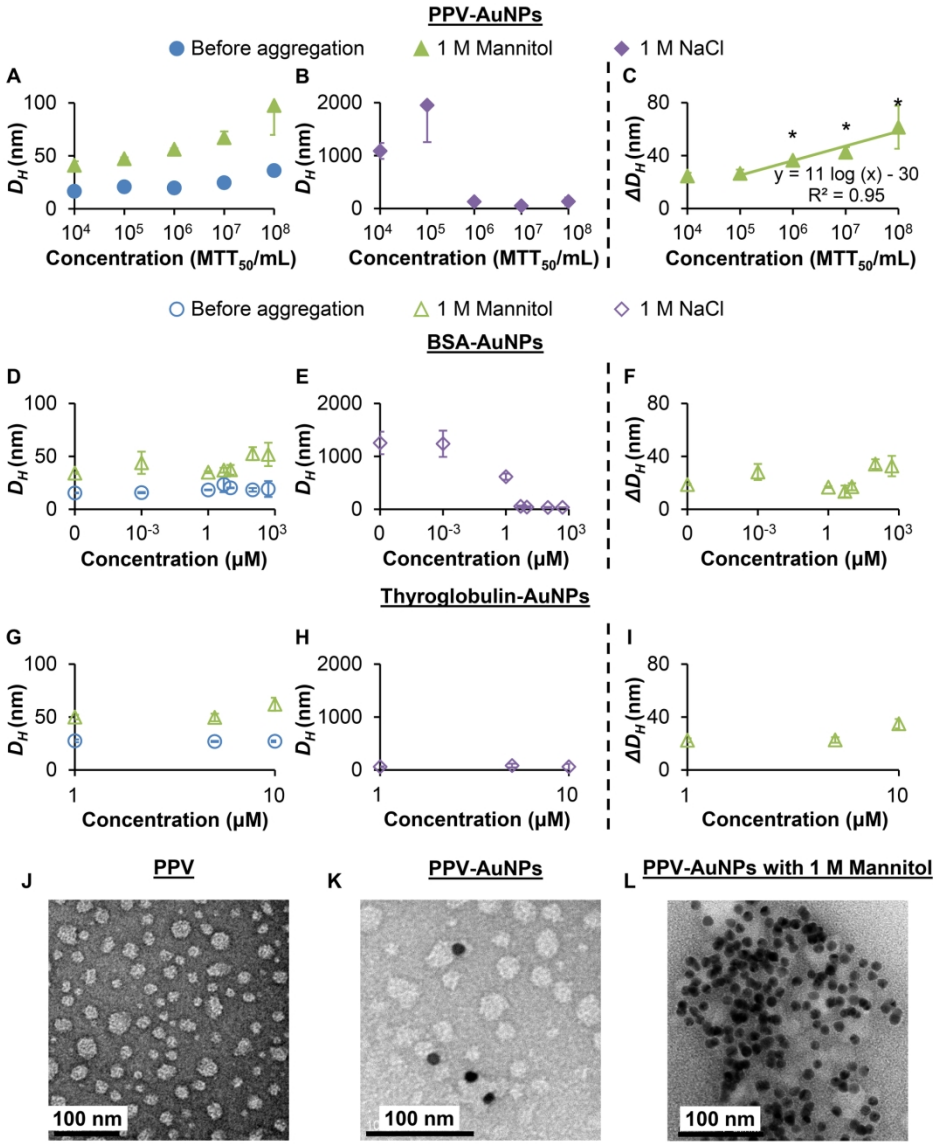

Figure 3 Concentration dependence for detection of PPV versus control BSA & thyroglobulin. (A&D&G) Size profile of PPV, BSA or thyroglobulin coated AuNPs as a function of concentrations before and after 1 M mannitol addition as measured by DLS. (B&E&H) Size profile of PPV, BSA or thyroglobulin coated AuNPs as a function of concentrations after 1 M NaCl addition as measured by DLS. (C&F&I) Change in AuNPs aggregation size for PPV, BSA or thyroglobulin after 1 M mannitol addition. Solid markers represent PPV, open markers represent BSA and thyroglobulin. All data points are the average of three separate tests and error bars represent the standard deviation. Concentrations are plotted as a log scale. TEM images of (J) 8 log PPV, (K) 8 log PPV-coated AuNPs and (L) 8 log PPV-coated AuNPs with 1 M mannitol. *p <0.05 for virus compared to BSA and thyroglobulin controls.

190x224mm (300 x 300 DPI)

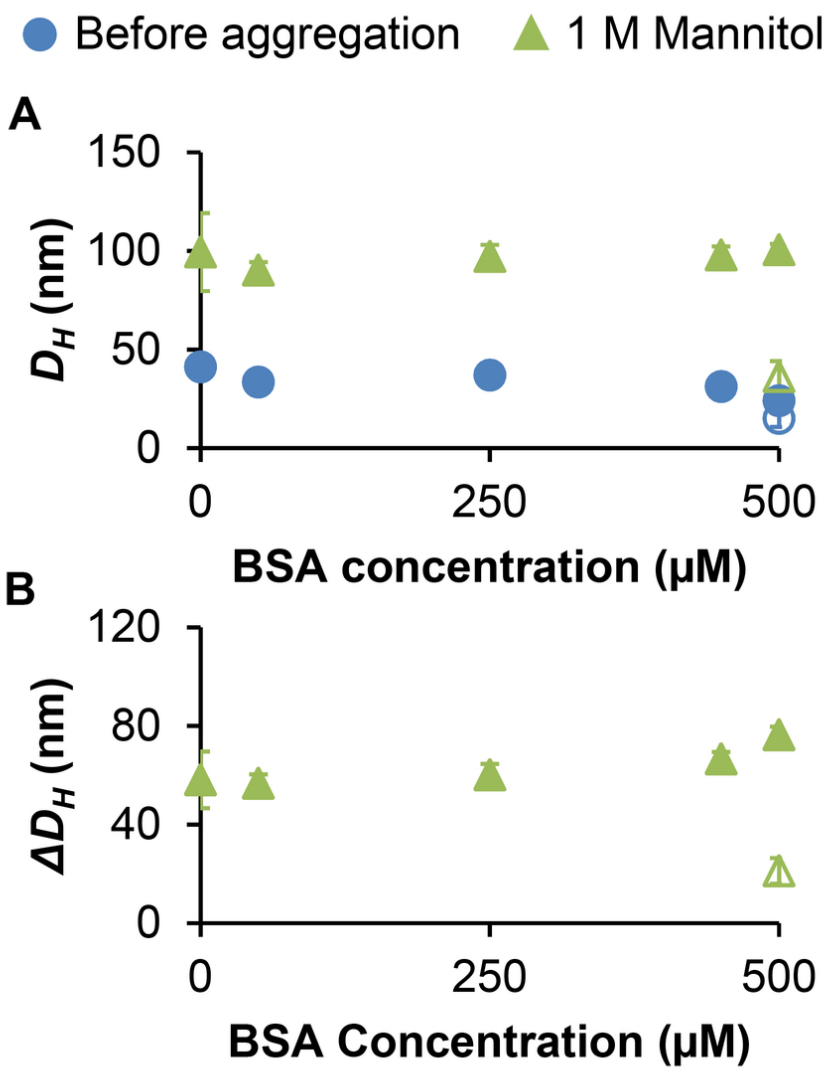

Figure 4 Detection of virus in a protein solution matrix. (A) The average size of PPV-coated AuNPs in different concentrations of BSA before and after 1 M mannitol addition and measured by DLS. (B) The change in the size of PPV-coated AuNPs in different concentrations of BSA after 1 M mannitol addition. Solid symbols represent PPV and open symbols represent BSA only. All data points are the average of three separate tests and error bars represent the standard deviation.

80x102mm (300 x 300 DPI)

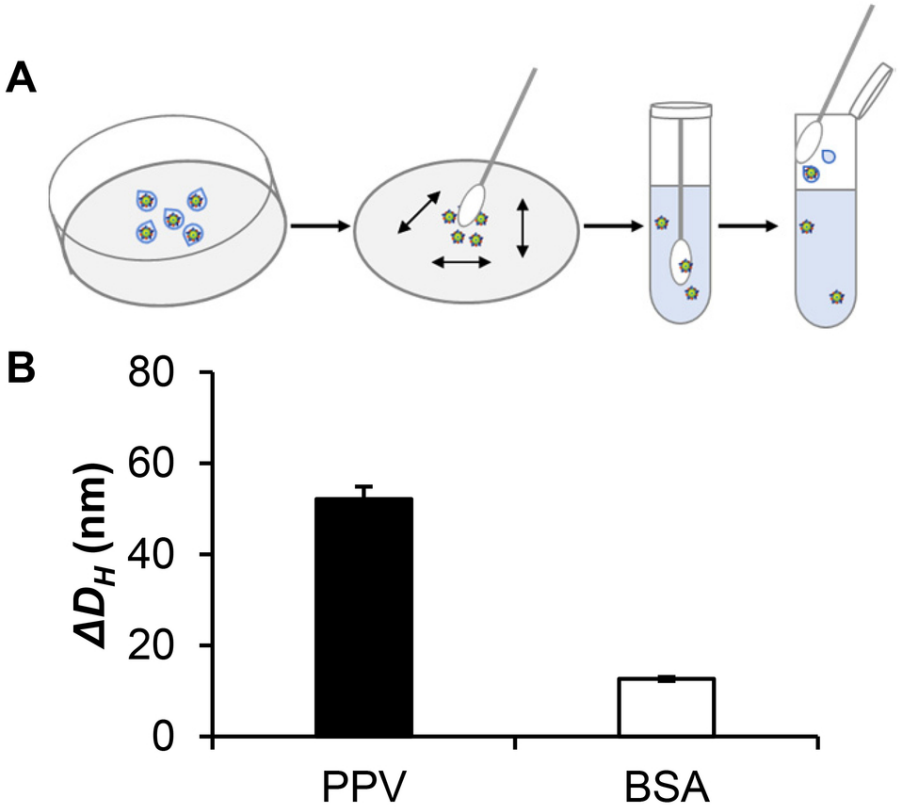

Figure 5 Swab sampling to detect contamination of PPV on a surface. (A) The process of swab sampling, (B) Size aggregation measured by DLS for swabbed PPV versus control swabbed BSA. Swabbed PPV is 10^6.9 ± 100.2 MTT50/mL as measured by the MTT assay and 10^7.4 MTT50/mL as measured by the PPV-AuNPs aggregation assay in 1 M mannitol. All data points are the average of three separate tests and error bars represent the standard deviation.

89x78mm (300 x 300 DPI)

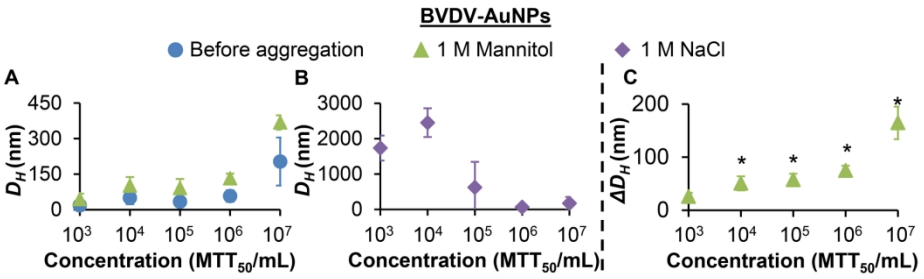

Figure 6 Concentration dependence for detection of BVDV. (A) Size profile of BVDV coated AuNPs as a function of concentrations before and after 1 M mannitol addition as measured by DLS. (B) Size profile of BVDV coated AuNPs as a function of concentrations after 1 M NaCl addition as measured by DLS. (C) Change in AuNPs aggregation size for BVDV after 1 M mannitol addition. All data points are the average of three separate tests and error bars represent the standard deviation. *p <0.05 for virus compared to BSA and thyroglobulin controls in Figure 3.

189x62mm (300 x 300 DPI)

Graphical Abstract

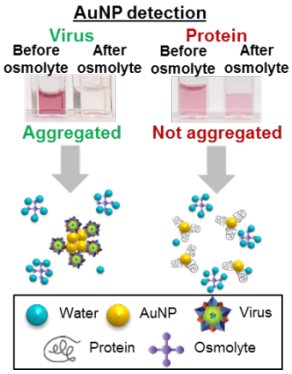

Addition of osmolytes causes viruses-coated AuNPs to aggregate and not protein-coated AuNPs. Ligand-free detection of virus was developed without the need for prior knowledge of the specific virus target.